AIP Physics of Plasmas

# Formation of a laminar electron flow for 300GHz high-power pulsed gyrotron

Yuusuke Yamaguchi, Yoshinori Tatematsu, Teruo Saito, Ryosuke Ikeda, Jagadish C. Mudiganti et al.

Citation: Phys. Plasmas **19**, 113113 (2012); doi: 10.1063/1.4768959

View online: http://dx.doi.org/10.1063/1.4768959

View Table of Contents: http://pop.aip.org/resource/1/PHPAEN/v19/i11

Published by the American Institute of Physics.

# Formation of a laminar electron flow for 300 GHz high-power pulsed gyrotron

Yuusuke Yamaguchi,[a] Yoshinori Tatematsu, Teruo Saito, Ryosuke Ikeda, Jagadish C. Mudiganti, Isamu Ogawa, and Toshitaka Idehara
*Research Center for Development of Far-Infrared Region, University of Fukui, 3-9-1 Bunkyo, Fukui-shi 910-8507, Japan*

(Received 6 August 2012; accepted 6 November 2012; published online 28 November 2012)

This paper describes the design of a triode magnetron injection gun for use in a 200 kW, 300 GHz gyrotron. As power and frequency increase, the performance of the gyrotron becomes quite sensitive to the quality of the electron beam. Formation of a laminar electron flow is essential for the realization of a high quality beam with a small velocity spread. In this study, a new method is developed for a quantitative evaluation of the laminarity and is applied to optimize the electrode design. The laminarity depends not only on conventional design parameters such as the cathode slant angle but also on the spatial distribution of the electric field along the beam trajectory. In the optimized design, the velocity pitch factors, $\alpha$, larger than 1.2 are obtained at 65 kV, 10 A with spreads, $\Delta\alpha$, less than 5%. © *2012 American Institute of Physics*.
[http://dx.doi.org/10.1063/1.4768959]

## I. INTRODUCTION

Gyrotrons are capable of providing high-power electromagnetic waves at millimeter and sub-millimeter wavelengths and are widely used in various fields for physics studies and for industrial and technological uses. Currently the most remarkable of these is the application to the study of plasma physics. In the field of nuclear fusion research, MW class tubes with frequencies from 28 to 170 GHz have been already utilized.[1–3] In the forthcoming years, development of a high power wave source in the sub-THz region is expected for the measurement of collective Thomson scattering (CTS) in the large helical device (LHD).[4,5] At Research Center for Far-Infrared Region (FIR Center), University of Fukui, development of a 295 GHz tube is currently in progress.[6,7] In this study, design of a magnetron-injection gun (MIG) is carried out using an electron trajectory code EGUN[8] to make a large current, laminar electron beam which is suitable for a new tube.

For use in the measurement of CTS in LHD, a high power source is required with a frequency less than several hundred GHz to ensure sufficient scattering angles for good spatial resolution. So far, a 77 GHz gyrotron for electron heating has been used for CTS diagnostics.[4,5] However, the application of such a low frequency presents difficulties in delivering the probe wave to a target plasma region because of refraction, cut-off, and absorption at the electron-cyclotron resonance layer. Additionally, signal detection is adversely affected by electron cyclotron emission (ECE) background noise. To avoid these disadvantages and to realize higher signal-to-noise ratios, the performance requirements are an oscillation frequency around 300–400 GHz, an output power of more than 100 kW, and a pulse duration of ~1 ms.[6,9–11]

At FIR Center, a high-power tube was initially developed using an 8 T superconducting magnet and a power supply with voltages up to 65 kV. The oscillation frequency was around 400 GHz at the second harmonic.[9–11] Although the single mode oscillation was successfully demonstrated with the world power record of the second harmonic gyrotrons, the power has remained around 85 kW.[6,11] Power saturation is observed as the beam current increases, which is likely due to deterioration of the beam quality.[11] Furthermore, the competing fundamental mode is found to prevent stable oscillation of the second harmonic mode. To achieve further increases in power with sufficient stability, it was decided to develop a new tube with a fundamental harmonic oscillation.[6,7] A cryogen-free 12 T superconducting magnet was introduced, and the design of the cavity has been performed with careful considerations for the oscillation mode, the frequency, and the beam-microwave coupling. Finally, we selected the frequency of 295 GHz with the cavity mode of $TE_{14,2}$. It is predicted by the simulation that a power of over 200 kW can be realized with a beam voltage $V_K$ of 65 kV, a current $I_B$ of more than 10 A, and the velocity pitch factor $\alpha$ (the ratio of perpendicular to parallel velocities to the magnetic field line) of 1.2 in the cavity.[6]

In gyrotrons, the electron gyration energy is transferred to the wave energy. For high power levels and efficiency, an intense beam is required with a larger $\alpha$ and smaller velocity spread. The spread of $\alpha$

$$\Delta\alpha \equiv (\alpha_{\text{maximum}} - \alpha_{\text{minimum}})/\alpha_{\text{average}} \quad (1)$$

should be minimized because it decreases the oscillation efficiency and may cause magnetic mirror reflections for a portion of the electrons.[12] Following the results of the 400 GHz gyrotron, special attention was paid to produce a high quality electron beam with a small velocity spread. Formation of a laminar electron flow is essential to obtain small velocity spreads, especially for large current beams.[3,13–16] The conventional design parameter has been the slant angle $\theta_E$ of the emission surface to the magnetic field line, which should be larger than 25° for a well laminated flow.[14–16] However,

[a]Electronic mail: y-yama@fir.u-fukui.ac.jp.

 

until now, no method has yet been reported to quantitatively evaluate laminarity in gyrotrons. In our latest work, a new method is proposed for evaluation of the laminarity and is applied to the MIG design.[10] Here, we consider the mechanism of a laminar flow formation from a fresh perspective which was found on the design process of the electrodes. It is found that $\theta_E$ has an optimum value, with which the highest laminarity and smallest velocity spread are obtained simultaneously. The optimum value of $\theta_E$ depends on the detailed shapes of the first anode and the cathode.[17] The shapes of the electrodes are carefully adjusted to form a laminar flow with small velocity spread in the region between the first anode and the cathode. The second anode is designed so as to maintain a minimal $\Delta\alpha$ value until the beam enters the cavity. Consequently we have obtained good electrode geometries, such that the $\Delta\alpha$ at the cavity entrance ($\Delta\alpha_{cavity}$) becomes quite small (less than 5%) for the averaged $\alpha$ at the cavity entrance ($\alpha_{cavity}$) of 1.2. The final MIG design has been applied to the fabricated 295 GHz, 200 kW pulsed gyrotron.

This paper is organized as follows: In Sec. II, we present the preliminary design of a MIG under various geometrical restrictions. After brief descriptions for the space charge effect, we present the formation of a laminar electron flow with the cathode and the first anode. The design of the second anode is also described. Section III is devoted to describe the performance of designed MIG and discussion. A summary is given in Sec. IV.

## II. DESIGN OF MIG

### A. Preliminary design

Beam quality is characterized by the spread, $\Delta\alpha$. Since the electron beam interacts with the transverse electric field in the cavity, the value of $\alpha_{cavity}$ should ideally be large with a minimized $\Delta\alpha_{cavity}$. In this study, beam simulation was conducted with EGUN, which allowed us to take into account the actual magnetic field distribution and electrode structure in the axisymmetric geometry.[8] Space charge and self-magnetic field effects were also included. To obtain accurate results, during the calculations the parameter values, such as mesh size, ray number, trajectory calculation step sizes, and the number of iterations, were monitored for validity. The mesh size was much smaller than the characteristic length for spatial distribution of the potential. The step size was short enough to describe the cyclotron motion. An adequate number of rays and iterations were determined such that convergence to a stationary solution was obtained within a realistic computation time.

Figure 1 gives a schematic drawing of the electrode design used for numerical computation of the beam trajectory. A typical trace of the beam trajectory is also shown. A triode-type structure is adopted to control the beam properties without changing the magnetic field and the total beam energy. The dimension of the MIG is restricted by the diameter of the room temperature 100 mm bore of the superconducting magnet. The MIG parameters were initially estimated from adiabatic theory. The radius of the cavity is 3.4 mm. To couple to the selected mode, $TE_{14,2}$, the electron

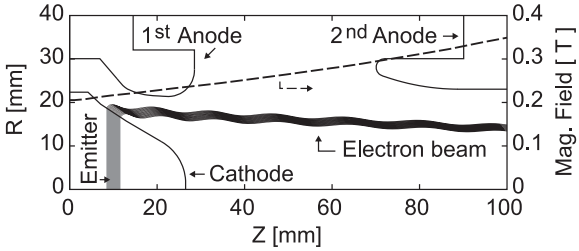


FIG. 1. Design of the electrodes used for the beam analysis. An example of the calculated beam trajectory is also shown.

beam should be injected into the cavity with a radius, $R_B$, of 2.42 mm. The axial distance of the emitter from the cavity was set at 535 mm after considering the limitation of 1260 mm tube length, the position of the output window, and the magnetic field profile. With this geometrical design, the magnetic compression ratio between the cavity and the emitter becomes $B_{cavity}/B_{emitter} = 53.2$. The radius of the emitting ring was evaluated at 17.6 mm, from which the guiding center of the electron arrives with $R_B = 2.42$ mm in the cavity. An axial extent of 3.2 mm was given for the annular thermionic-emitter strip to ensure a small guiding center spread in the cavity, which is required for strong oscillation of a single mode and to keep cathode loading below several $A/cm^2$ for a reasonable emitter life time. Moreover, because of the small size, the electric terminal insulation structures outside the vacuum region have to be compact. To provide enough electrical insulation, the voltage between the cathode and the first anode ($V_{KA}$) is limited to 30 kV. The distance between the cathode and the first anode of 6.5 mm is derived from conditions where the expected $\alpha_{cavity}$ of 1.2 is obtained with a $V_{KA}$ smaller than 25 kV.

To optimize the electrode designs, the beam trajectories were calculated for various electrode shapes. We have performed an integrated study to minimize $\Delta\alpha_{cavity}$. Furthermore, in a small electron gun, the beam properties may show great sensitivity to small changes in the electrodes. We confirmed that with the final design, $\Delta\alpha_{cavity}$ was relatively insensitive to misalignments and fabrication errors of the electrodes.

### B. Space charge effect and necessity of laminar flow

With large beam currents, local concentration of the space charge has a strong effect on $\Delta\alpha$. To reduce the influence of the space charge, formation of a laminar flow becomes important. Figures 2 and 3 show typical calculation results for different $\theta_E$ of 12° and 28°, respectively. Depending on the $\theta_E$, the axial extent of the emitter is adjusted to keep the same cathode loading and beam radius in the cavity. The axial profiles of the beam trajectory, the space charge density, and the $\Delta\alpha$ are illustrated in each figure. The cavity center is located at $z = 545$ mm. The beam voltage $V_K$ and the current $I_B$ are 65 kV and 10 A, respectively. In all cases, the first anode potential is adjusted so that $\alpha_{cavity}$ is maintained at 1.2.

For $\theta_E = 12°$ (Fig. 2), the spatial distances between the neighboring trajectories are not uniform. Therefore, the space charge concentrates periodically at the locations

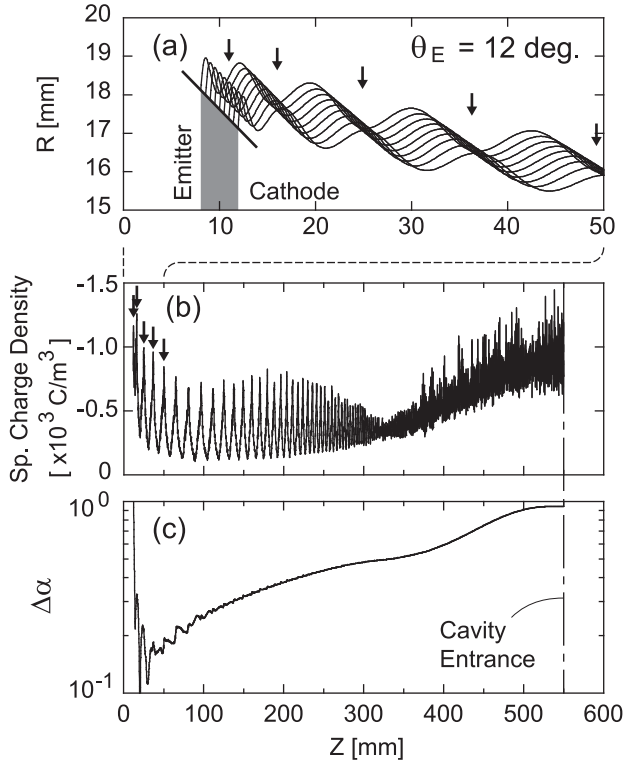


FIG. 2. The result of the beam analysis for $\theta_E = 12°$. Axial profiles of (a) beam trajectories, (b) space charge density, and (c) $\Delta\alpha$.

indicated by the vertical arrows. Then, the electric field which arises from the inhomogeneous space charge distribution perturbs strongly the motions of the electrons. It is seen in Figs. 2(b) and 2(c) that $\Delta\alpha$ becomes increasingly large

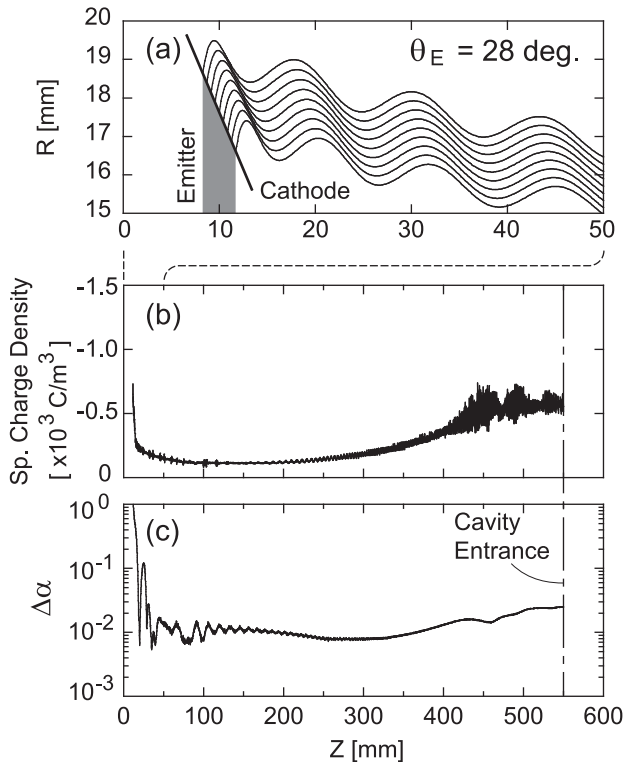


FIG. 3. The result of the beam analysis for $\theta_E = 28°$. Axial profiles of (a) beam trajectories, (b) space charge density, and (c) $\Delta\alpha$.

with changes in the space charge density and reaches a value near 95% at the cavity.

On the other hand, no local concentration of the space charge occurs when $\theta_E = 28°$ (Fig. 3), and space charge forces are weak. The resultant $\Delta\alpha$ remains small (less than 5%) until the beam arrives at the cavity. When compared with the $\theta_E = 12°$ case, the trajectories are distributed uniformly, i.e., the laminarity is high. Therefore, the formation of a laminar electron flow is essential to avoid deterioration of beam properties caused by space charge forces.

### C. Formation of laminar flow

The objective for a new MIG design is creation of a laminar beam to reduce $\Delta\alpha_{cavity}$ while keeping a large value of $\alpha_{cavity}$. To realize a well laminated flow, the conventional method is to increase the $\theta_E$. The critical angle, at which laminarity disappears, is thought to be $\theta_E = 25°$.[14–16] For a detailed investigation of laminar flow formation, a quantitative evaluation of the laminarity is needed. However, no method has been reported for quantitative evaluation of the laminarity in MIGs. In this study, a formula to quantify the laminarity is defined as follows:[7]

$$d(z) = \frac{1}{N-1}\sum_{j=1}^{N-1}\left|\frac{r(z)_{j+1} - r(z)_j}{w(z)/(N-1)} - 1\right|,$$
$$F_{laminar} \equiv \frac{1}{L}\int_L \frac{1}{1+d(z)}dz, \tag{2}$$

where $N$ is the number of the trajectories used for the calculation and $r_j$ represents the radial position of the $j$-th trajectory numbered from the innermost trajectory. Each variable in Eq. (2) corresponds to the one in Fig. 4. The thickness $w$ of the beam at the axial position $z$ is estimated from the difference between the outermost and innermost guiding-center radii which are traced from both ends of the emitter. In an ideal laminar flow, the trajectories are distributed uniformly. The parameter $d(z)$ represents the degree of deviation from the ideal condition where all the trajectories are placed with equally spaced intervals. The more $d(z)$ increases, the stronger the space-charge force perturbs the electron velocity. The changes in the electron velocity accumulate through the beam path and result in an increase in the $\Delta\alpha_{\text{cavity}}$. To take into account this accumulation effect, laminarity is expressed by integration of a term composed of $d(z)$. If $d(z)$ is zero over the axial length $L$ from the emitter edge to the cavity entrance, the value of $F_{\text{laminar}}$ becomes unity.

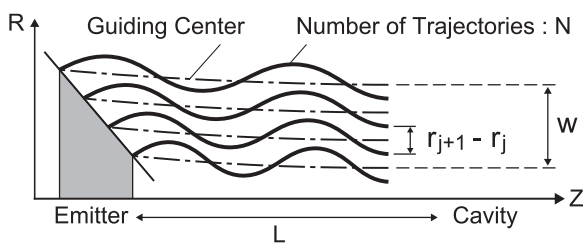


FIG. 4. Parameters used in the laminarity evaluation defined.

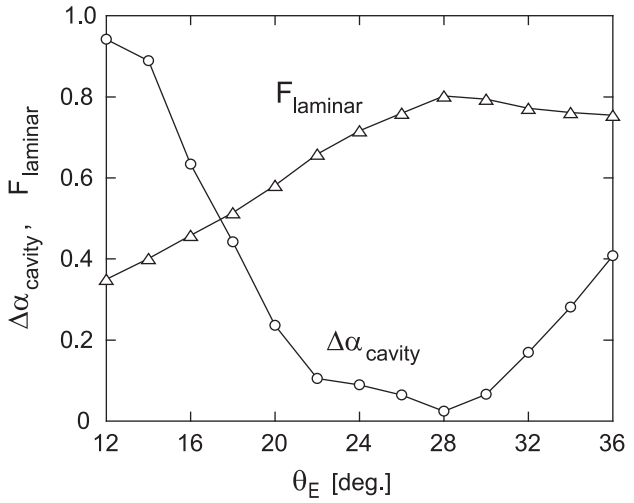


FIG. 5. Variations of $F_{laminar}$ and $\Delta\alpha_{cavity}$ are given as a function of $\theta_E$ for the case of $V_K = 65\,\text{kV}$, $I_B = 10\,\text{A}$. By changing the $V_{KA}$, the $\alpha_{cavity}$ is fixed at 1.2.

Figure 5 shows the variations of $F_{laminar}$ and $\Delta\alpha$ at the cavity, given as a function of $\theta_E$. In the calculations of the values shown in the figure, the applied voltage $V_{KA}$ is adjusted at each point so that the $\alpha_{cavity}$ is always kept at 1.2. The calculated laminarity is closely connected to $\theta_E$. At $\theta_E = 28°$, $F_{laminar}$ is maximized and the resultant $\Delta\alpha_{cavity}$ reaches a minimum. Here, the value of $\theta_E$ is finally set at 28°. It is found that $\theta_E$ has an optimum value, where maximum laminarity and minimum $\Delta\alpha_{cavity}$ values are realized. This result indicates that formation of the laminar flow is not determined by simply increasing the slant angle $\theta_E$.

On the other hand, $\Delta\alpha_{cavity}$ increases rapidly while $F_{laminar}$ varies little at $\theta_E$ larger than 28°. It is obvious that the thickness $w$ increases with $\theta_E$, and hence the space-charge density becomes small. As a result, the sensitivity of $\Delta\alpha_{cavity}$ on $F_{laminar}$ is expected to be weak for large $\theta_E$. Therefore, this rapid change in $\Delta\alpha_{cavity}$ suggests that additional factors play a role in determining $\Delta\alpha$. Some modifications to Eq. (2) are necessary to obtain a more precise description of the laminarity.

To discover additional factors that influence the laminarity and $\Delta\alpha$, we have focused on the variation of $\alpha$ for each trajectory. Traces of the beam trajectories and their pitch factor for $\theta_E = 28°$ are shown in Fig. 6. Between the cathode and the first anode, the $\alpha$ for each trajectory changes considerably. To see the relationship between variations of $\alpha$ and the laminarity, the axial variation in each $\alpha$ value and the corresponding trajectory are illustrated schematically in Fig. 7. The corresponding $\alpha$ (Fig. 7(a)) and the trajectory (Fig. 7(b)) are indicated with the same line styles. It is revealed that $\alpha$ values of the inner trajectory are always larger than those of the outer one at each axial point. Thus, electrons on the outer trajectory travel a longer distance than electrons on the inner trajectory within each cycle of cyclotron motion. Then, the phase differences between the rotating trajectories become small, and a well laminated flow is formed. The resultant space charge distribution is almost uniform, and hence local concentration of the charge disappears. In the region of $z > 70\,\text{mm}$, it is seen that each trajectory has almost the same $\alpha$, which means $\Delta\alpha$ is quite small. The $\Delta\alpha$ remains small until the beam enters the cavity.

Therefore, formation of a well laminated flow depends not only on the slant angle $\theta_E$ but also on the adjustment of the axial pitch of the cyclotron motion. The $\alpha$ of each trajectory is modified with the spatial distribution of the electric field, which is determined by the shapes of the cathode and the first anode.

### D. Design of the second anode

The initial beam velocity is controlled by the electric field in the vicinity of the emitter surface. $\Delta\alpha$ can be minimized by shaping the cathode and the first anode. After leaving the region between the cathode and the first anode, the electron trajectory is also perturbed by the electric field formed by the second anode. Sometimes an electrostatic lens may actively be immersed in the region between the first and the second anodes for additional adjustment of the beam properties.[14,16] However, if the second anode is far enough away from the beam and the first anode that the electric field is homogeneous, the influence of spatial variation of the electric field on $\Delta\alpha$ will be negligible. In this study, a laminar beam with small $\Delta\alpha$ is formed without using the lens effect. The second anode is designed to have negligible effects on $\Delta\alpha$ before the cavity. Consequently, optimization of the cathode and the first anode design can be separated from that of the second anode.

As given in Fig. 8, we used the radius RA and the axial distance DA from the emitter as the main design parameters for the second anode. In Fig. 8, $\Delta\alpha_{cavity}$ is plotted as a function of RA and DA. As RA and DA increase, $\Delta\alpha_{cavity}$ decreases, and its sensitivity to RA and DA becomes weak. Moreover, an increase in DA also causes some degree of rise

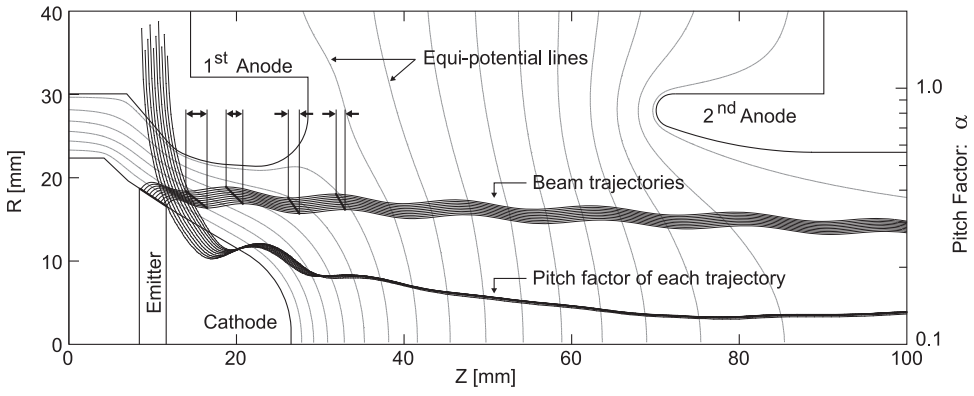


FIG. 6. Axial distributions of representative beam trajectories and the corresponding $\alpha$ values for $\theta_E = 28°$. The averaged value of $\alpha$ becomes 1.2 at the cavity (z = 545 mm).

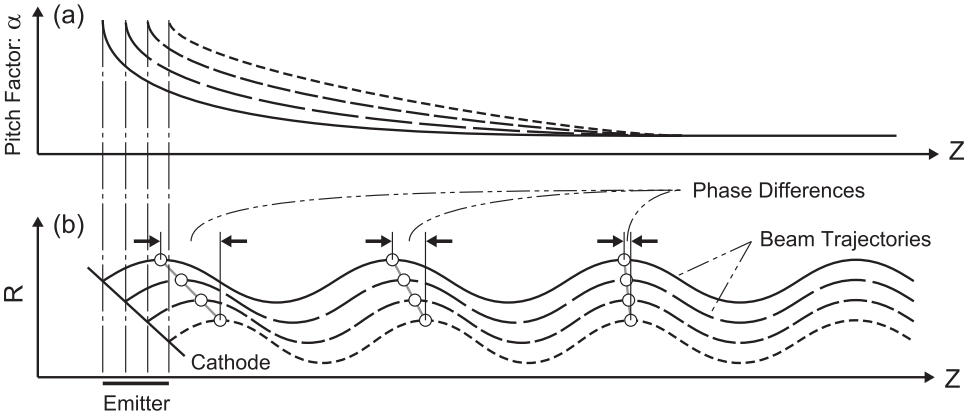


FIG. 7. The relationship between the variations in α and the laminarity.

and fall in $\Delta\alpha_{cavity}$. This oscillatory change in $\Delta\alpha_{cavity}$ is attributed to the cyclotron motion of the beam. As DA is increased, the spatial distance of the second anode entrance from the beam is changed not only by the beam radius but also by the rotating phase of the cyclotron motion. As the second anode is further separated from the beam, $\Delta\alpha_{cavity}$ settles at lower values (see Fig. 8(b)).

On the other hand, taking into account the installation of a water cooling circuit inside the second anode, RA should be as small as possible. Furthermore, the maximum value of DA is restricted by the structure of the insulator installed between the first and the second anodes. Final selected values were RA = 23 mm and DA = 60 mm, with which the $\Delta\alpha_{cavity}$ is kept low with higher stability for changes in RA and DA.

## III. OVERALL PERFORMANCE OF DESIGNED MIG

We have modified the shapes of the cathode and the first anode to maximize $F_{laminar}$. In this process, differences in the gyration phases shown in Fig. 7(b) were used as a useful figure of merit. The design optimization resulted in a minimized $\Delta\alpha_{cavity}$ as well as a wide operation window of the MIG. In Fig. 9(a), $\alpha_{cavity}$ and $\Delta\alpha_{cavity}$ are plotted as a function of $V_{KA}$. No mirror reflection of the electrons occurs over the entire voltage range from 23 to 28 kV. The desired value of the $\alpha_{cavity}$ of 1.2 was realized even at beam currents larger than 20 A. Since the laminarity is quite high, deterioration of the $\Delta\alpha_{cavity}$ caused by rises in $I_B$ is small. In all cases, small $\Delta\alpha_{cavity}$ values less than 5% have been achieved in the expected operating region of $\alpha_{cavity} = 1.0$–$1.3$. The $\alpha_{cavity}$ value decreases with increasing beam current $I_B$ because of the voltage depression caused by the space charge between the cathode and the first anode. In Fig. 9(b), the $\alpha_{\text{cavity}}$ and the $V_{KA}$ are plotted versus the electric field in the vicinity of the emitter surface $E_{emitter}$ for different $I_B$ values. As indicated with solid curves, regardless of their $I_B$, the $\alpha_{cavity}$ values lie on almost the same curve for changes in the $E_{emitter}$. When $I_B$ is increased, the voltage depression becomes large. Therefore, the required $V_{KA}$ increases with $I_B$ to obtain a certain value of $E_{emitter}$, as plotted with dashed lines.

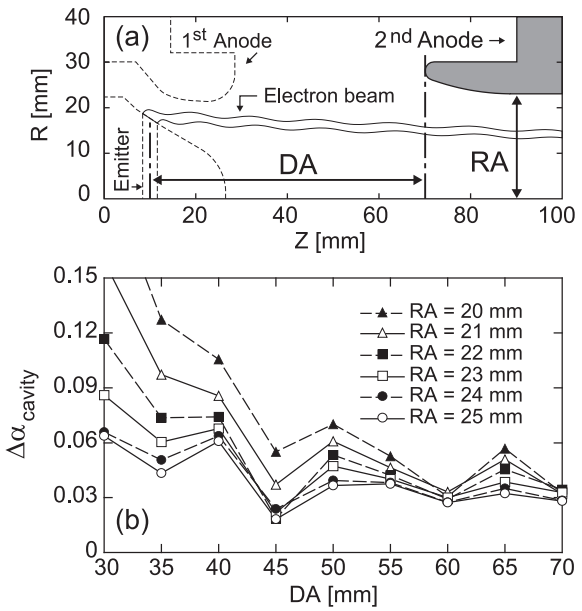


FIG. 8. (a) Configuration of second anode. (b) Variations of $\Delta\alpha$ at the cavity and $V_{KA}$ are given as functions of RA and DA for the case of $V_K = 65$ kV, $I_B = 10$ A. By changing $V_{KA}$, $\alpha_{cavity}$ is fixed at 1.2.

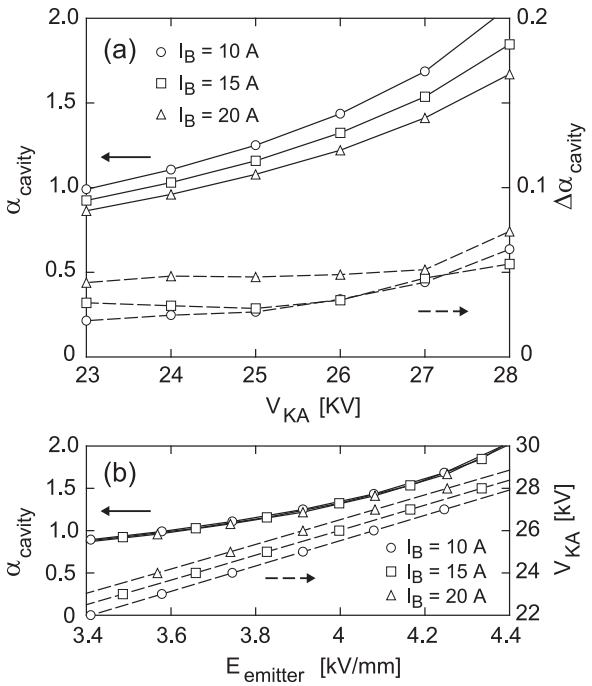


FIG. 9. (a) Calculated $\alpha_{cavity}$ and $\Delta\alpha_{cavity}$ for $V_K = 65$ kV, $I_B = 10$–$20$ A electron gun. (b) Voltage depression in the vicinity of the emitter surface.

The peak electric field of $E_{emitter} = 4.4\,\mathrm{kV/mm}$ is low enough to avoid arcing. For the desired pitch factor of $\alpha_{cavity} = 1.2$, $E_{emitter}$ becomes 3.78 kV/mm. The extracted current of 10 A corresponds to cathode loading of $2.26\,\mathrm{A/cm^2}$. This value is approximately 10% of the space charge limited current. Those values satisfy the performance requirements to avoid strong influences of the space charge on the beam properties.[16]

Another important factor which strongly influences the beam quality is roughness of the emitter surface. Due to the absence of accurate data for the surface roughness, the effect of initial velocity spread at the emitter was neglected in the simulations. After the manufacturing process of the cathode, the roughness was measured using an optical microscope as $\sim 4\,\mu\mathrm{m}$ on average. By use of a simple model in which a hemisphere on the emitter plane is assumed to describe the roughness, spread in the velocity perpendicular to the magnetic field line can be approximately estimated with a formula[12]

$$\Delta v_{\perp} = 1.6\sqrt{\left(1+\frac{\pi^2}{4}\tan^2\theta_E\right)\frac{r}{h}}. \tag{3}$$

Here, $r$ is the radius of the hemisphere and $h$ is the height of the first maximum of the electron trajectory above the cathode. In case of $V_k = 65\,\mathrm{kV}$, $I_b = 10\,\mathrm{A}$, and $\alpha_{\mathrm{cavity}} = 1.2$, the value of $h$ becomes $\sim 1.5\,\mathrm{mm}$. Then, $\Delta v_{\perp}$ is calculated as $\sim 10\%$ which corresponds to $\Delta\alpha_{\mathrm{cavity}} \sim 30\%$. This result indicates that the emitter surface roughness possibly introduces a more significant velocity spread as compared with the space-charge effect. However, even if the spread calculated with Eq. (3) is simply superposed to the one calculated with EGUN code, the value of $\Delta\alpha_{cavity}$ is still small enough to keep stability and to avoid mirror reflection of the beam.[18] For more rigorous estimation, a detailed model which allows for the influence of the surface roughness should be adopted.[13,19]

## IV. SUMMARY

The design of a MIG for a 295 GHz, 200 kW gyrotron was carried out with EGUN. To realize an intense, laminar electron beam, a method was developed for the quantitative evaluation of laminarity. Formation of a well laminated flow depends not only on the slant angle $\theta_E$ but also on the spatial distribution of the electric field along the beam. In a well laminated beam, the axial pitch of each helical motion is modified so that every electron in the plane perpendicular to the field line has almost the same gyro-radius and almost the same phase of gyration after passing between the cathode and the first anode. The second anode is shaped to keep $\Delta\alpha$ minimized until the beam enters the cavity. An electron gun which is suitable for the new gyrotron has been successfully designed.

## ACKNOWLEDGMENTS

The authors would like to thank the members in FIR FU for their fruitful discussions. The present study is partly supported by programs of Grants-in-Aid for Scientific Research of Japan Society for the Promotion of Science.

[1]K. Sakamoto, A. Kasugai, Y. Ikeda, K. Hayashi, K. Takahashi, S. Moriyama, M. Seki, T. Kariya, Y. Mitsunaka, T. Fujii, and T. Imai, Nucl. Fusion **43**, 729 (2003).
[2]M. Thumm, Int. J. Infrared Millim. Waves **26**, 483 (2005).
[3]T. Kariya, R. Minami, T. Imai, M. Ota, Y. Endo, S. Kubo, T. Shimozuma, H. Takahashi, Y. Yoshimura, S. Ito, T. Mutoh, K. Sakamoto, and Y. Mitsunaka, J. Infrared Millim. Terahertz Waves **32**, 295 (2011).
[4]M. Nishiura, K. Tanaka, S. Kubo, T. Saito, Y. Tatematsu, T. Notake, K. Kawahata, T. Shimozuma, and T. Mutoh, Rev. Sci. Instrum. **79**, 10E731 (2008).
[5]S. Kubo, M. Nishiura, K. Tanaka, T. Shimozuma, Y. Tatematsu, T. Notake, T. Saito, Y. Yoshimura, H. Igami, H. Takahashi, and N. Tamura, Plasma Fusion Res. **5**, S1038 (2010).
[6]N. Yamada, T. Saito, Y. Tatematsu, S. Ikeuchi, Y. Yamaguchi, R. Ikeda, I. Ogawa, T. Idehara, S. Ogasawara, S. Kubo, T. Shimozuma, K. Tanaka, M. Nishiura, and V. N. Manuilov, in *Proceedings of the 4th International Workshop on Far-Infrared Technologies 2012*, Fukui, 2012, edited by Y. Tatematsu (University of Fukui, Japan, 2012), p. 228.
[7]Y. Yamaguchi, Y. Tatematsu, T. Saito, R. Ikeda, J. C. Mudiganti, I. Ogawa, and T. Idehara, Plasma Fusion Res. **7**, 1205004 (2012).
[8]W. B. Herrmannsfeldt, SLAC-331-UC-28, 1998.
[9]T. Notake, T. Saito, Y. Tatematsu, S. Kubo, T. Shimozuma, K. Tanaka, M. Nishiura, A. Fujii, La Agusu, I. Ogawa, and T. Idehara, Rev. Sci. Instrum. **79**, 10E732 (2008).
[10]T. Notake, T. Saito, Y. Tatematsu, A. Fujii, S. Ogasawara, La Agusu, I. Ogawa, and T. Idehara, Phys. Rev. Lett. **103**, 225002 (2009).
[11]T. Saito, N. Yamada, S. Ikeuti, S. Ogasawara, Y. Tatematsu, R. Ikeda, I. Ogawa, T. Idehara, V. N. Manuilov, T. Shimozuma, S. Kubo, M. Nishiura, K. Tanaka, and K. Kawahata, Phys. Plasmas **19**, 063106 (2012).
[12]Sh. E. Tsimring, Radiophys. Quantum Electron. **15**, 952 (1972).
[13]A. N. Kuftin, V. K. Lygin, V. N. Manuilov, A. S. Postnikova, and V. E. Zapevalov, Int. J. Infrared Millim. Waves **20**, 361 (1999).
[14]P. V. Krivosheev, V. K. Lygin, V. N. Manuilov, and Sh. E. Tsimring, Int. J. Infrared Millim. Waves **22**, 1119 (2001).
[15]Sh. E. Tsimring, Int. J. Infrared Millim. Waves **22**, 1433 (2001).
[16]V. N. Manuilov, T. Idehara, T. Saito, La Agusu, T. Hayashi, and I. Ogawa, Int. J. Infrared Millim. Waves **29**, 1103 (2008).
[17]K. T. Nguyen, B. G. Danly, B. Levush, M. Blank, R. True, G. R. Good, T. A. Hargreaves, K. Felch, and P. Borchard, IEEE Trans. Plasma Sci. **26**, 799 (1998).
[18]V. N. Manuilov and S. A. Polushkina, Radiophys. Quantum Electron. **52**, 714 (2009).
[19]V. K. Lygin, Int. J. Infrared Millim. Waves **16**, 363 (1995).